

A calorimetric study of precipitation in commercial aluminium alloy 6061

I. DUTTA, S. M. ALLEN

Materials Science Group, Department of Mechanical Engineering, Naval Postgraduate School, Monterey, CA 93943, USA

Differential scanning calorimetry (DSC) is a well-established technique which is often utilized to characterize precipitate microstructures and kinetics rapidly in age-hardenable aluminium alloys [1-4]. Recently, DSC has also been used to study the effect of reinforcement on the ageing kinetics of various aluminium matrix composites [5, 6]. The microstructural changes accompanying DSC peaks in 2xxx and 7xxx series aluminium alloys are well characterized [1-4]. However, no detailed calorimetric study of precipitation in 6xxx series aluminium alloys has been reported to date. In this study, transmission electron microscopy (TEM) has been utilized in conjunction with DSC to study precipitate evolution in aluminium alloy 6061.

5.5 mm diameter, 1.5 mm thick discs were machined from commercial aluminium alloy 6061 plates, solutionized at 813 K for 1.5 h in argon atmosphere and quenched in ice-water at 273 K. The discs were then analysed immediately in a Perkin-Elmer 2C DSC from 273 to 833 K using a heating rate of 10 K min⁻¹. In addition to the solutionized and quenched samples, samples pre-aged for 1.5 h at 298 and 313 K were also analysed. The data from each run were transformed into differential heat capacity (ΔC_p) versus temperature by subtracting a baseline representing the C_p of the alloy with its existing precipitates. The baseline was obtained by scanning a sample aged for 72 h at 473 K (overaged) from 273 to 800 K and extrapolating the

plot to 833 K. For TEM observation of the microstructures associated with various peaks, 3 mm discs were heated in the DSC to the requisite temperatures at 10 K min⁻¹ and immediately cooled to 273 K at 320 K min⁻¹. The samples were then thinned by electropolishing in a solution of 3% perchloric acid, 62% ethanol and 35% butoxy-ethanol at 233 K and examined under a Jeol 100CX-TEM at an accelerating voltage of 120 kV. Any interim storage before observation was done at liquid-nitrogen temperature.

Fig. 1 shows the thermogram of the solutionized and quenched alloy. Four exothermic formation peaks, including one at 355 K (a), two partially overlapping peaks close to 515 K (b) and 565 K (c), and one at 767 K (d) are apparent, followed by an endothermic dissolution peak at 820 K (e). A close observation of Fig. 1 suggests that peak b is an unresolved doublet consisting of two superimposed peaks. The data from the superposed intermediate temperature peaks were deconvoluted using a non-linear regression procedure described in [7]. The result is shown in Fig. 2, where peak b is seen to consist of two separate exotherms b1 and b2.

Fig. 3 shows the TEM micrograph of a sample heated to 400 K to reveal the precipitates corresponding to peak a. A high density of tiny (about 1.0 nm) precipitates are observed. The corresponding $[001]_{Al}$ selected-area diffraction pattern (SADP) shows no additional feature, indicating that

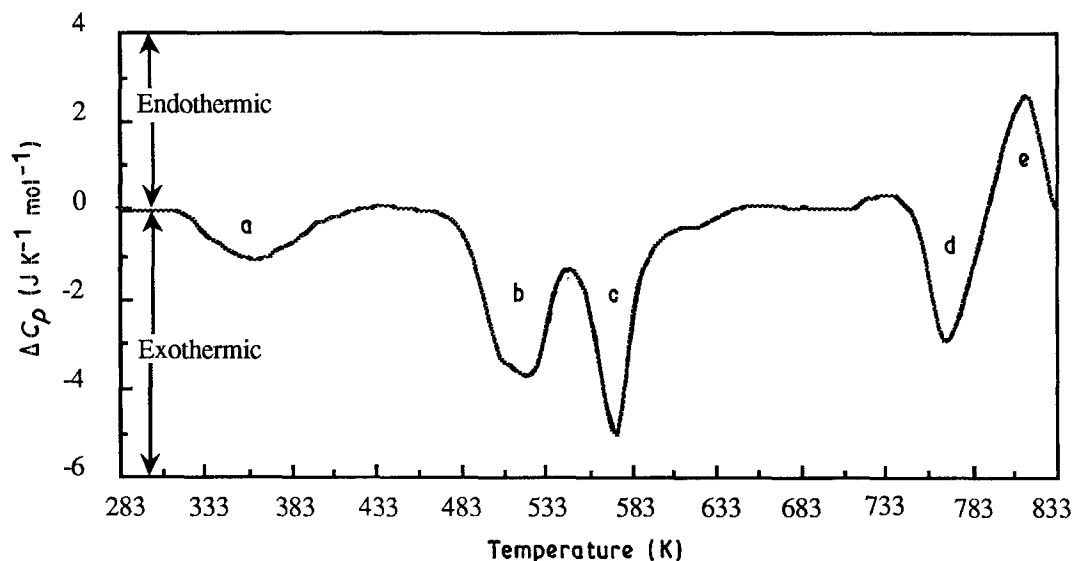


Figure 1 DSC thermogram (scan rate 10 K min⁻¹) of solutionized and quenched 6061 Al, showing four precipitate formation peaks, a through d, and one dissolution peak, e.

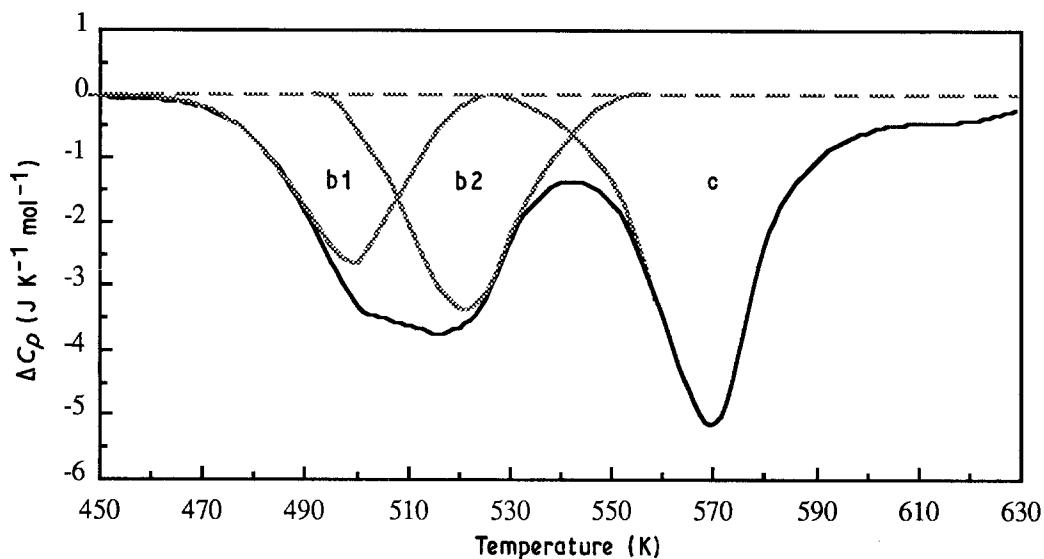


Figure 2 Part of the DSC thermogram of the solutionized and quenched alloy, showing peaks b and c after deconvolution. Peak b is seen to consist of two unresolved exotherms, b1 and b2.

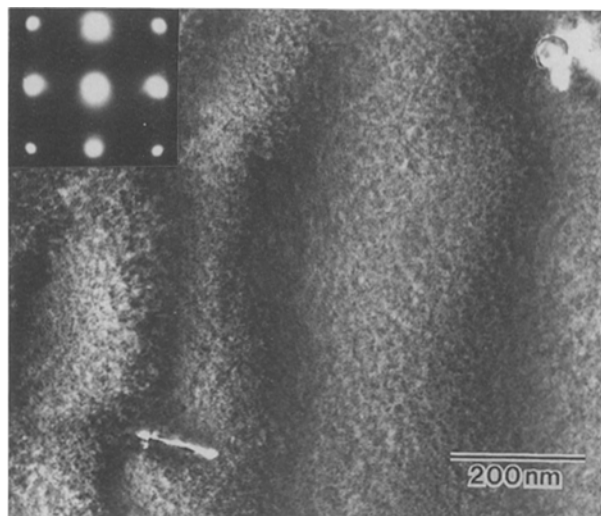


Figure 3 Centred dark-field (g_{200}) TEM micrograph of the alloy heated to 400 K at 10 K min^{-1} after solutionizing and quenching to reveal the precipitate structure corresponding to peak a. A high density of small Si clusters is observed.

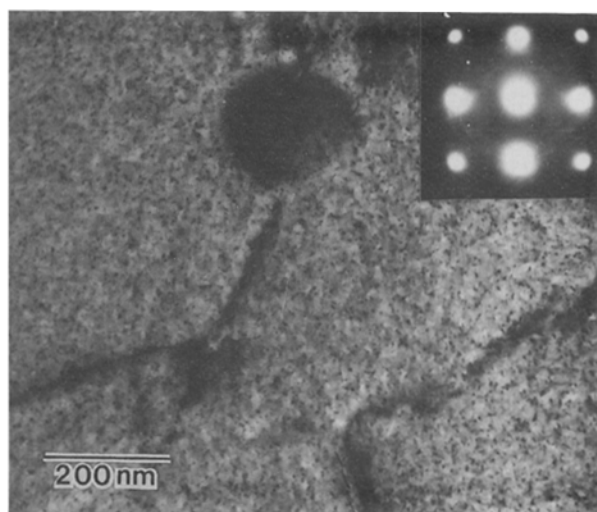


Figure 4 Microstructure corresponding to DSC peak b1, showing small "dot-like" precipitates of unresolved shapes. These precipitates were identified to be GP-I zones. Some needles causing faint streaks in the SADP are also observed. The particle in the micrograph is an intermetallic arising from alloy impurities.

the precipitates are fully coherent with the matrix and are visible only due to strain contrast. The image characteristics of these precipitates were found to be similar to those corresponding to silicon precipitation at quenched-in vacancy-clusters in Al–Si alloys [8]. The initial stage of ageing in Al–Mg–Si alloys is known to be similar to that in Al–Si alloys [9, 10], suggesting that peak a is associated with the formation of Si clusters.

Fig. 4 reveals the precipitates corresponding to peak b1 in a sample heated to 505 K. The bright field (BF) micrograph (zone axis $[001]_{\text{Al}}$) reveals strain contrast due to two kinds of precipitates. Most of the precipitates appear as tiny dots about 2.5 nm in diameter, whereas a few are short, thin needles oriented along $[010]_{\text{Al}}$ and $[100]_{\text{Al}}$. Some of the dots might be needles viewed end-on, but the majority are very small precipitates with unresolved shapes. The SADP reveals faint streaks along $\langle 100 \rangle_{\text{Al}}$, representative of the few needle-like precipitates [11–14]. The faint rings in the SADP are

due to contaminants. Therefore, the sample heated to 505 K (middle of peak b1) consists of mostly dot-like and some needle-like precipitates.

Fig. 5a shows the BF micrograph of a sample heated to 515 K (middle of peak b2). It is seen that the principal precipitate is needle-shaped (about 15.0 nm long and 4.0 nm in diameter). Prominent $\langle 100 \rangle_{\text{Al}}$ streaks are visible in the corresponding SADP. In the dark field (CDF) image with strong $g = \bar{2}00$ (Fig. 5b), one variant of the needles (those with their axes parallel to $g = \bar{2}00$) is found to disappear. This suggests that the precipitates are coherent with the matrix and are visible due to a strain field perpendicular to the needle axes, which produces the streaks in the SADP. The needle-like precipitate shape might also contribute to streaking, although not very strongly, as suggested by the absence of streaking of the transmitted spot. Since $\{100\}$ reflections are forbidden in fcc, the $\langle 100 \rangle_{\text{Al}}$ streaks suggest the presence of order in the precipitates [12]. The intensity modulation along the streaks

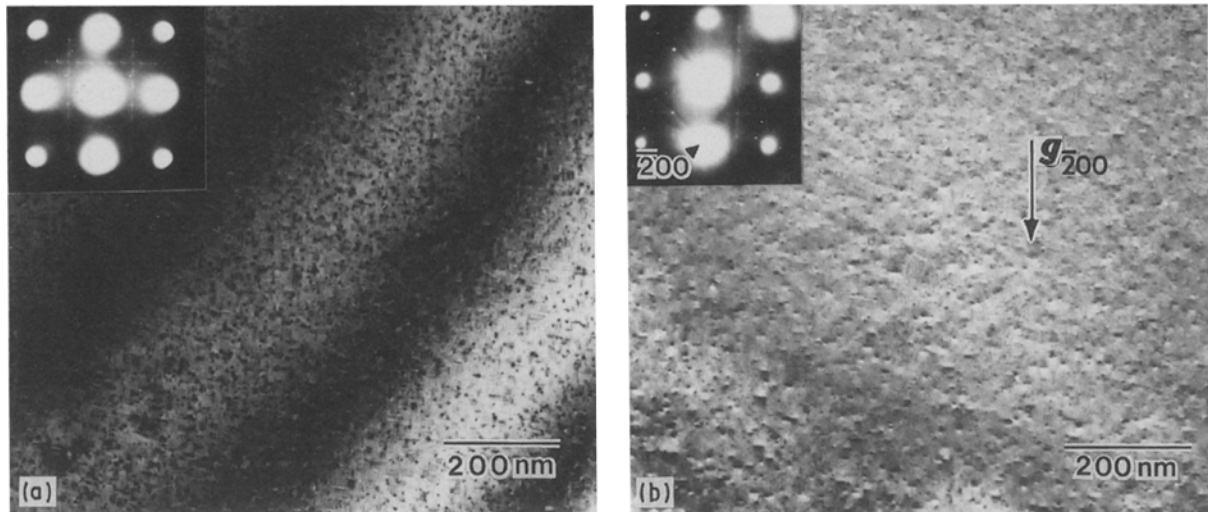


Figure 5 (a) Needle-like GP-II zone (β'') precipitates corresponding to DSC peak b2. Note the presence of $\langle 100 \rangle_{\text{Al}}$ streaks with lengthwise intensity modulations in the SADP. (b) Centred dark-field (strong g_{200}) TEM micrograph of the same sample showing the disappearance of the needles parallel to g_{200} . This suggests the existence of a matrix strain field along $[200]$, i.e. perpendicular to the needle axes.

is attributable to precipitate order perpendicular to the needle axes [13]. Thus the DSC exotherm b2 represents the formation of an ordered, at least partially coherent, needle-shaped phase.

Due to the superposition of the b1 and b2 peaks and the relatively slow quench rate (320 K min^{-1}) attained in the DSC, it is probable that the limited number of needles observed in Fig. 4 were from the b2 peak, whereas the dots were due to b1. Therefore, it is proposed that peak b1 represents the formation of very tiny GP-I zones of unresolved shapes, whereas peak b2 represents the formation of ordered, needle-shaped GP-II zones (or β''). Although it is generally believed that GP zones in Al-Mg-Si alloys are needle-like [11–15], Cordier and Gruhl [16] observed approximately spherical GP zones, whereas Smith [17] observed a duplex precipitate morphology consisting of both spherical and needle-like GP zones in the peak-aged alloy. Based on the results of this study, it is clear that the near-spherical precipitates observed by other investigators correspond to GP-I zones, and the needle-

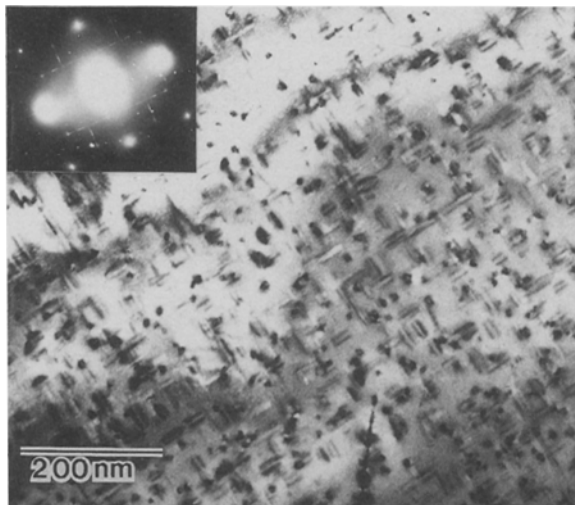


Figure 6 Bright-field TEM micrograph showing rod-shaped β' precipitates associated with the DSC exotherm c and the corresponding SADP.

like precipitates correspond to GP-II zones.

Fig. 6 shows the BF micrograph and the corresponding $[001]_{\text{Al}}$ SADP of a sample heated to 600 K (end of peak c). The GP-II needles have grown into rods which are about 5.0–7.5 nm in diameter and 50.0 nm in length. Because of the large length-to-diameter ratio of the precipitates, a shape effect is now discernible, as evident from the $\langle 100 \rangle_{\text{Al}}$ streaking of the transmitted spot. In addition, faint streaks through the $\{200\}$ spots with lengthwise intensity modulations similar to those corresponding to the hexagonal rod-shaped phase identified in [14] are also visible. These rod-like precipitates correspond to the transition β' - Mg_2Si [11, 12, 17], and hence peak c represents β' formation. A sample heated to 760 K was also examined under the TEM and, as expected [5, 6], incoherent platelets of equilibrium β - Mg_2Si were observed to grow from β' rods, indicating that the exotherm d represents β formation. The final endothermic peak e represents the dissolution of β .

Fig. 7 shows the initial part of the DSC thermograms of the solutionized and quenched alloy, as well as after pre-ageing for 1.5 h at 298 and 313 K. Two features of the thermograms are noteworthy. First, the Si-cluster formation exotherm shifts to higher temperatures with progressive pre-ageing, concurrent with an increase in the associated activation energy (E_a) and the free energy of activation (ΔG_a) (Table I). This is attributable to a decrease in the number of vacancy loops available for nucleation of Si-clusters due to coalescence and growth during pre-ageing. Secondly, the GP-I zone formation peak disappears on pre-ageing, whereas the GP-II zone (β'') exotherm becomes enlarged, indicating that pre-ageing supports the formation of GP-II zones directly from Si-clusters without going through the intermediate GP-I zone. This suggests that the formations of GP-I and GP-II zones are parallel, competitive processes. If they were sequential events, the disappearance of the GP-I zone exotherm

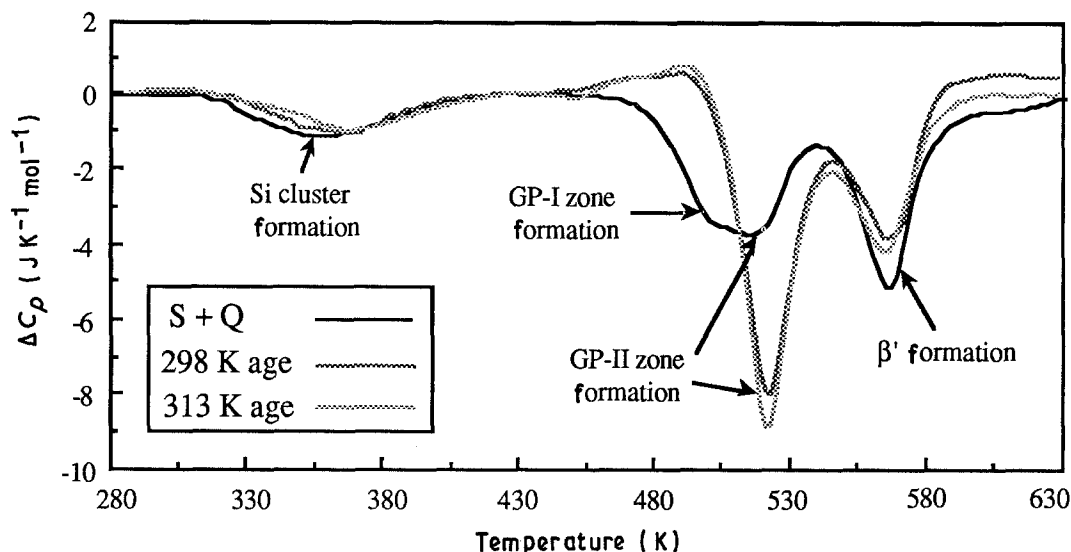


Figure 7 The effect of pre-ageing for 1.5 h at 298 and 313 K on the DSC thermogram of 6061 Al. With pre-ageing the Si-cluster formation peak shifts to higher temperatures, the GP-I zone formation peak disappears and the GP-II zone peak is enlarged.

TABLE I Peak temperature (T_p), Arrhenius activation energy (E_a) and free energy of activation (ΔG_a) for silicon-clustering at vacancy loops in 6061 Al. E_a and ΔG_a were calculated from the DSC data using the absolute reaction rate theory per [1].

Heat treatment	T_p (K)	E_a (kJ mol ⁻¹)	ΔG_a (kJ mol ⁻¹)
Solutionized and quenched	355	33.10 ± 7.5	103.1 ± 6.2
Pre-aged 1.5 h at 298 K	363	43.70 ± 11	104.4 ± 4.0
Pre-aged 1.5 h at 313 K	369	46.44 ± 13	105.1 ± 4.6

would be expected only if the peak due to Si-clustering were also absent. Since a relatively short pre-ageing treatment causes the needle-like GP-II zones to form directly from Si-clusters, care has to be exercised to prevent ageing between the solutionize-quench treatment and the subsequent heat treatment in order to obtain GP-I zones. This might explain why GP-I zones were not observed in several previous studies [11–15].

In conclusion, the DSC exotherms representing precipitation processes in 6061 Al were found to be associated with vacancy-silicon clusters (peak a), GP-I zones having unresolved shapes (peak b1), needle-like GP-II zones or β'' (peak b2), rod-like β' (peak c) and plate-shaped β -Mg₂Si (peak d), respectively. It was found that pre-ageing retards Si-clustering and favours the formation of GP-II (β'') over GP-I zones, which form competitively from Si-clusters.

Acknowledgements

The authors gratefully acknowledge the many helpful discussions with Professors T. Yamashita, A. G.

Fox and K. Sengupta. This work was supported by the NPS Research Council.

References

1. R. DEIASI and P. N. ADLER, *Met. Trans.* **8A** (1977) 1177.
2. P. N. ADLER and R. DEIASI, *ibid.* **8A** (1977) 1185.
3. J. M. PAPAIZIAN, *ibid.* **12A** (1981) 269.
4. J. M. PAPAIZIAN, R. J. DEIASI and P. N. ADLER, *ibid.* **11A** (1980) 135.
5. J. M. PAPAIZIAN, *ibid.* **19A** (1988) 2945.
6. I. DUTTA and D. L. BOURELL, *Mater. Sci. Engng.* **A112** (1989) 67.
7. R. F. SPEYER, B. C. RICHARDSON and S. H. RISBUD, *Met. Trans.* **17A** (1986) 1479.
8. E. OZAWA and H. KIMURA, *Mater. Sci. Engng.* **8** (1971) 327.
9. I. KOVACS, J. LENDVAI and E. NAGY, *Acta Metall.* **20** (1972) 975.
10. S. CERESARA, E. DI RUSSO, P. FIORINI and A. GIARDA, *Mater. Sci. Engng.* **5** (1969–70) 220.
11. H. J. RACK and R. W. KRENZER, *Met. Trans.* **8A** (1977) 335.
12. G. THOMAS, *J. Inst. Metals* **90** (1961–2) 57.
13. D. W. PASHLEY, J. W. RHODES and A. SENDOREK, *ibid.* **94** (1966) 41.
14. M. H. JACOBS, *Phil. Mag.* **26** (1972) 1.
15. A. LUTTS, *Acta Metall.* **9** (1961) 577.
16. H. CORDIER and W. GRUHL, *Z. Metallkde* **56** (1965) 669.
17. W. F. SMITH, *Met. Trans.* **4** (1973) 2435.

Received 2 July
and accepted 21 August 1990